Crystal structure, Raman scattering and magnetic properties of CuCr2– xZrxSe4 and CuCr2– xSnxSe4 selenospinels

C. Pinto, A. Galdámez, P. Barahona, S. Moris, O. Peña

Crystal structure, Raman scattering and magnetic properties of CuCr$_{2-x}$Zr$_x$Se$_4$ and CuCr$_{2-x}$Sn$_x$Se$_4$ selenospinels

C. Pinto[a], A. Galdámez[a*], P. Barahona[b*], S. Moris[c] and O. Peña[d]

[a] *Departamento de Química, Facultad de Ciencias, Universidad de Chile, Santiago, Chile*

[b] *Facultad de Ciencias Básicas, Universidad Católica del Maule, Talca, Chile*

[c] *Vicerrectoría de Investigación y Postgrado, Universidad Católica del Maule, Talca, Chile*

[d] *Institut des Sciences Chimiques de Rennes, UMR 6226, Université de Rennes 1, Rennes, France*

ABSTRACT

Selenospinels, CuCr$_{2-x}$M$_x$Se$_4$ (M = Zr and Sn), were synthesized *via* conventional solid-state reactions. The crystal structure of CuCr$_{1.5}$Sn$_{0.5}$Se$_4$, CuCr$_{1.7}$Sn$_{0.3}$Se$_4$, CuCr$_{1.5}$Zr$_{0.5}$Se$_4$, and CuCr$_{1.8}$Zr$_{0.2}$Se$_4$ were determined using single-crystal X-ray diffraction. All the phases crystallized in a cubic spinel-type structure. The chemical compositions of the single-crystals were examined using energy-dispersive X-ray analysis (EDS). Powder X-ray diffraction patterns of CuCr$_{1.3}$Sn$_{0.7}$Se$_4$ and CuCr$_{1.7}$Sn$_{0.3}$Se$_4$ were consistent with phases belonging to the $Fd\bar{3}m$ space group. An analysis of the vibrational properties on the single-crystals was performed using Raman scattering measurements. The magnetic properties showed a spin glass behavior with increasing Sn content and ferromagnetic order for CuCr$_{1.7}$Sn$_{0.3}$Se$_4$.

* Corresponding authors: e-mail pbaraho@ucm.cl (PB), agaldamez@uchile.cl (AG)

1. Introduction

Colossal magnetoresistance (CMR) is the considerable change in electrical resistance experienced by certain materials due to the presence of a magnetic field [1]. This physical property is currently of great scientific interest due to its technological applications for the development of new data storage devices with lower energy requirements [2,3]. Over the last two decades, perovskite manganites have been well studied, mainly focused on their magnetoresistance [4,5]. However, in most cases, this property only occurs at very high magnetic fields, which greatly restricts their use as magnetic field sensors [6].

CMR effect has been observed in chromium-based chalcogenide materials with spinel structures, ACr_2Q_4 (A = transition metal, Q = S, Se) [3,7], e.g., Cu- and Cr- based systems, $CuCr_2S_4$, $CuCr_2Se_4$ and $CuCr_2Te_4$, which are metallic and ferromagnetic with Curie temperatures (T_C) of ~380, ~420, and ~300 K, respectively [8-10]. The magnetism in these compounds can be attributed to the double exchange between Cr^{3+} and Cr^{4+} [8]. These compounds crystallize in a normal spinel structure (space group $Fd\bar{3}m$), and the Cu and Cr ions occupy the tetrahedral A and octahedral B sites, respectively. In these compounds, the cations from the A and B sites can be substituted by other cations without changing the structure. However, the physical properties of the substituted compound can differ from those of the non-substituted compound.

Several studies on $CuCr_{2-x}M_xQ_4$ spinels revealed that whereas copper exists as the diamagnetic Cu^+ cation the M atoms array exist in the 4+ oxidation state (M = Ti, Zr, Hf), thus changing the properties of the original material [11-15]. Thus, the chemical substitutions of chromium in $CuCr_2Se_4$ end-member by M^{4+} cations play an important role in the particular magnetic/electrical properties of these compounds. Sn^{4+} and Zr^{4+} cations, in oxidation state 4+ (diamagnetic behavior), modify overall the magnetic contribution of the chromium sublattice producing also an octahedral distortion.

The present work describes the solid state synthesis of $CuCr_{2-x}Zr_xSe_4$ ($x = 0.2$ and 0.5) and $CuCr_{2-x}Sn_xSe_4$ ($x = 0.3$, 0.5, and 1.0) phases, their crystal structures, Raman characterization and magnetic properties. These materials are prospective candidates for spin-based electronic (spintronic) applications because the strong interaction between the electronic and spin subsystems results in drastic changes in the electronic transport and optical properties near the Curie temperature T_C.

2. Experimental

2.1. Synthesis

$CuCr_{2-x}Zr_xSe_4$ and $CuCr_{2-x}Sn_xSe_4$ compounds were prepared by directly combining high-purity elemental powders (99.99 %, Aldrich) in stoichiometric amounts. All manipulations were carried out under argon atmosphere. The reaction mixtures were sealed in evacuated quartz ampoules and placed in a programmable furnace. The ampoules were then slowly heated at a rate of 1°C/min, from room temperature until 400°C, followed by a heating-rate of 2.5°C/min up to the maximum temperature of 950°C for $CuCr_{2-x}Zr_xSe_4$ and 850°C for $CuCr_{2-x}Sn_xSe_4$, and held for 6 days. Finally, the ampoules were slowly cooled to room temperature at a rate of 1°C/min. Single crystals were obtained for $CuCr_{1.5}Sn_{0.5}Se_4$, $CuCr_{1.7}Sn_{0.3}Se_4$, $CuCr_{1.5}Zr_{0.5}Se_4$, and $CuCr_{1.8}Zr_{0.2}Se_4$ and polycrystalline materials for $CuCr_{1.7}Sn_{0.3}Se_4$ and $CuCr_{1.3}Sn_{0.7}Se_4$.

2.2 Crystal structure determination

XRD data for $CuCr_{1.5}Sn_{0.5}Se_4$, $CuCr_{1.7}Sn_{0.3}Se_4$ and $CuCr_{1.8}Zr_{0.2}Se_4$ were collected at room temperature using a Bruker Kappa CCD diffractometer with MoKα radiation, $\lambda = 0.71073$ Å. Data collection, data reduction and cell refinement: Bruker SMART (Bruker 2000) [16]. Multi-scan absorption correction was performed with SADABS program [17]. XRD data for $CuCr_{1.5}Zr_{0.5}Se_4$ were collected at room temperature using a Bruker AXS D8-Venture diffractometer with Cu Kα radiation, $\lambda = 1.54178$ Å. Data collection, cell refinement and data reduction: APEX3 (Bruker,

2016) [18]. Multi-scan Absorption correction for absorption anisotropy was performed [19]. Program used to refine the crystal structures: SHELXL (Sheldrick, 2015) [20] and Olex2 (Dolomanov et al., 2009) [21]. Software used to prepare the material for publication: PLATON (Spek, 2003) [22]. The refined occupation factors of Cr and M were consistent with the energy-dispersive X-ray chemical EDS analyses. The CIF files were deposited in the FIZ Karlsruhe database (76344 Eggenstein-Leopoldshafen, Germany; e-mail: crysdata@fiz-karlsruhe.de; fax: (49)7247–808–666). The depository numbers are CSD-433161 for $CuCr_{1.5}Sn_{0.5}Se_4$, CSD-433162 for $CuCr_{1.7}Sn_{0.3}Se_4$, CSD-433163 for $CuCr_{1.5}Zr_{0.5}Se_4$, and CSD-433164 for $CuCr_{1.8}Zr_{0.2}Se_4$.

2.3 Powder X-ray diffraction

Powder X-ray diffraction (PXRD) patterns were collected at room temperature on a Bruker D8 Advance diffractometer equipped with a Cu Kα radiation source ($\lambda = 1.5406$ Å); samples were scanned in the range $5° < 2\theta < 80°$.

2.4 SEM-EDS analysis

The chemical compositions of the samples were determined via energy-dispersive X-ray analysis using a Bruker Vega 3 Tescan system equipped with a Quantax 400 (EDS) microanalyzer. Samples were mounted on double-sided carbon tape, which was adhered to an aluminum holder.

2.5. Raman spectroscopy

The Raman spectra of the single crystals were recorded in the frequency range 50 -1800 cm^{-1} using a micro-Raman Renishaw system 1000 equipped with a Leica-DMLM microscope. The spectra data were collected at room temperature with a laser line of 633 nm and a laser power of ~1 mW.

2.6 Magnetic measurements

Magnetic measurements were performed on pelletized powder samples using a Quantum Design MPMS XL5 SQUID susceptometer. The magnetic nature of the material was determined using ZFC/FC (zero-field-cooled/field-cooled) cycles at low fields (typically 500 Oe).

3. Results and Discussion

3.1 Crystal structure analysis

The crystal structures of $CuCr_{1.5}Sn_{0.5}Se_4$, $CuCr_{1.7}Sn_{0.3}Se_4$, $CuCr_{1.5}Zr_{0.5}Se_4$, and $CuCr_{1.8}Zr_{0.2}Se_4$ were resolved by single-crystal X-ray diffraction (Fig. 1). The least-squares refinement of the occupation factors and displacement parameters converged on a model in which the tetrahedral positions were occupied by Cu (8a sites) and the octahedral positions (16d sites) were occupied by M (M = Sn, Zr) and Cr. The Se atoms occupy the 32e (u,u,u) sites in a closely packed cubic array. The refined occupation factors of the octahedral sites were 16d = $(2-x)$Cr + xM, and these were consistent with the EDS chemical analysis. The M and Cr atoms were constrained to identical displacement parameters. The detailed crystallographic data and refinement results for the single crystals are summarized in Table 1. The atomic coordinates and equivalent isotropic displacement parameters are listed in Table 2.

The lattice parameter a for all of the single crystals obeyed Vegard's law (Fig. 2). The lattice parameters of $CuCr_2Se_4$ (10.337 Å), $CuCrZrSe_4$ (10.669 Å) and $CuCrSnSe_4$ (10.672 Å) end-members were also included [23-25]. As expected, the cell parameters expanded due to the substitution of Cr $[Cr^{3+}/Cr^{4+}]$ by the larger Zr^{4+} and Sn^{4+} cations. The effective octahedral ionic radii of the Cr^{3+}, Cr^{4+}, Zr^{4+} and Sn^{4+} cations published by Shannon (for a high-spin configuration) are 0.62 Å, 0.55 Å, 0.72 Å and 0.69 Å, respectively [26]. The chemical compositions of the single crystals used in the X-ray diffraction experiments were examined using SEM-EDS. The backscattered image and EDS mapping analysis

(chemical maps of several areas) revealed homogenous single crystals in the scanned region (Fig. 3 shows, as an example, the case of $CuCr_{1.8}Zr_{0.2}Se_4$).

The Cu-Se distances in $CuCr_{2-x}Zr_xSe_4$ are 2.368(9) Å ($x = 0.2$) and 2.3839(8) Å ($x = 0.5$). The Cu-Se distances compare well with those found in cubic $CuCr_{2-x}Ti_xSe_4$ (2.3701 to 2.3716 Å) [11]. In both $CuCr_{1.8}Zr_{0.2}Se_4$ and $CuCr_{1.5}Zr_{0.5}Se_4$ compounds, the bond distances of (Cr/Zr)-Se (2.538(12) to 2.5557(5) Å, respectively) are consistent with the bond length in cubic $CuCrZrSe_4$ (2.614 Å) [25]. For $CuCr_{2-x}Sn_xSe_4$ ($x = 0.3$ and 0.5), the Cu-Se distances are 2.3832(6) Å, 2.3947(6) Å, respectively. In this case, the bond distances of (Cr/Sn)-Se are 2.5458(3) Å, and 2.5671(4) Å , respectively.

The bond angles of Se-(Cr/Zr)-Se (180.0°, 92.97° and 87.03°) in $CuCr_{1.5}Zr_{0.5}Se_4$ are very similar to the bond angles in $CuCr_{1.5}Ti_{0.5}Se_4$ (180.0°, 93.17°, and 86.83°) [11]. The crystal structure has a three-atom centered polyhedral unit, $CuSe_4$ (tetrahedron), $(Cr/Zr)Se_6$ (octahedron) and $Se[M_3Cu]$ (tetrahedron). In the tetrahedron, the Se atom is coordinated by one Cu and three metal atoms, M (M = Cr/Zr). The bond angles of (Cr/M)-Se-Cu in the tetrahedral $Se[M_3Cu]$ are distorted from those in an ideal tetrahedron. The degree of distortion in the polyhedral can be measured using the edge length distortion (ELD) indices [27-29]. The $Se[M_3Cu]$ tetrahedron is the most distorted polyhedron (~ 8 % distortion from an ideal tetrahedron). These values compare very well with those found for $CuCr_{2-x}Ti_xSe_4$ [11].

3.2 Raman scattering

From a vibrational point of view, the irreducible representations of the optical phonon modes in the $CuCr_2Se_4$ spinel-type crystal structure (space group $Fd\overline{3}m$) can be written as $\Gamma = A_{1g} + E_g + F_{1g} + 3F_{2g} + 2A_u + 2E_u + 5F_{1u} + 2F_{2u}$ [30]. The A_{1g}, E_g, and F_{2g} modes are Raman-active with five peaks in the Raman spectrum. The A_{1g} and E_g vibrations correspond to a symmetric radial breathing and a tangential displacement, respectively. These vibrational modes represent the expansion or contraction of the Cu-Se

bonds which are triggered by the displacement of the Se atoms in the vertices of the tetrahedron. Otherwise, the decomposition of the permutational representations for the 16d (Cr, M) and 32e (Se) positions results in $\Gamma = A_{1g} + F_{2g}$. These modes for the Se displacements have identical radial components relative to those of Cr and M (M = Zr, Sn).

Fig. 4 shows the Lorentzian fits for the Raman spectra of single crystals of $CuCr_{2-x}Zr_xSe_4$ (x = 0.2 and 0.5) and $CuCr_{2-x}Sn_xSe_4$ (x = 0.5) between ~70 to 300 cm^{-1}. The frequencies of the peaks are consistent with the main Raman peaks reported for single crystals of $CuCr_2Se_4$ and $CdCr_2Se_4$ (end-member) [30,31].

The Raman spectrum of $CuCr_{1.8}Zr_{0.2}Se_4$ (Fig. 4b) has two main peaks at 136 and 215 cm^{-1} assigned to the E_g and A_{1g} vibration modes, which are analogous to the $CuCr_2Se_4$ peaks [30]. In addition, the spectrum has two peaks at 98 cm^{-1} and 163 cm^{-1} that are assigned to the F_{2g} mode. The Raman spectra show the variations in the frequencies of all the vibration modes, ~10 cm^{-1}, together with a decrease in the intensity of the F_{2g} mode. The symmetrical stretching of the A_{1g} mode in $CuCr_2Se_4$ appears at 227 cm^{-1}, whereas for $CuCr_{1-x}Zr_xSe_4$, the values are 215 cm^{-1} for x = 0.2 and 252 cm^{-1} for x = 0.5. In contrast, in $CuCr_{1-x}Sn_xSe_4$, the values are 262 cm^{-1} for x = 0.5 (Fig. 4c). The displacement of the signals depends on the Cr chemical substitution.

The third mode, F_{2g}, appears at 220 cm^{-1} in $CuCr_2Se_4$. In $CuCr_{1-x}Zr_xSe_4$, the values are 202 cm^{-1} for x = 0.2 and 232 cm^{-1} for x = 0.5, and in $CuCr_{1-x}Sn_xSe_4$, the values are 244 cm^{-1} for x = 0.5. This third signal, F_{2g}, is very important because its intensity increases as a function of the quantity of the metal substitution. The growth in the intensity of F_{2g} far exceeded the growth in the intensity of the A_{1g} band, and this is related to the amount of Zr and Sn added to the structure and polarizability. Indeed, Fajans [32] indicates that an element with an incomplete external electron shells, e.g., Sn^{4+}, has a higher polarizability than an element with a noble gas configuration, e.g., Zr^{4+}, and higher than Cr^{3+}; this

electronic arrangement causes distortion, resulting in a higher band intensity. Moreover, the displacement is related to the complexity of the movement and is coupled to the bending of the Se-Cu-Se angle, and this may be because the angle of the Cu-Se-M bond (M = Cr, Zr, and Sn) tends to swell (122.80°, 122.94° and 123.44°, respectively).

3.3 Magnetic properties on polycrystalline materials

Besides the single-crystal data thoroughly discussed above, some Sn-based and Zr-based samples were prepared as polycrystalline materials in large enough quantities to characterize their magnetic behavior. As mentioned in the Experimental section (§.2.1), $CuCr_{1-x}Sn_xSe_4$ compounds were prepared at a maximum temperature of 850 °C whereas $CuCr_{1-x}Zr_xSe_4$ samples were synthesized at 950 °C. The Powder X-ray diffraction (PXRD) patterns of $CuCr_{1.7}Sn_{0.3}Se_4$ and $CuCr_{1.3}Sn_{0.7}Se_4$ were fully indexed in the $Fd\bar{3}m$ space group (spinel-type structure) and compared with the simulated XRD patterns derived from the single-crystal XRD data (Fig S1 and Fig S2, Supporting Information). Jendrzejewska et *al.* proposed that $CuCr_{2-x}Sn_xSe_4$ phases had a tetragonal crystal structure of $I4_1/amd$ space group, as refined by Rietveld techniques [33], whereas our experimental data on single-crystals showed that the $CuCr_{1.5}Sn_{0.5}Se_4$ and $CuCr_{1.7}Sn_{0.3}Se_4$ phases belonged to the cubic $Fd\bar{3}m$ spinel structure-type. Trials to synthesize large quantities of polycrystalline Zr-based materials were, however, unsuccessful since their PXRD patterns and SEM-EDS analysis showed that the reaction products of nominal composition $CuCr_{1-x}Zr_xSe_4$ were not single phases, being composed of $CuCr_{1-x}Zr_xSe_4$, $ZrSe_3$ and some unidentified impurities (Fig S3 and Fig S4, Supporting Information). For this reason, only the Sn-based samples were characterized by their magnetic properties, as discussed below.

The ZFC/FC magnetization cycles for the $CuCr_{2-x}Sn_xSe_4$ ($x = 0.3$ and 0.7) samples, performed under low magnetic fields (500 Oe), are shown in Fig. 5 and Fig 6. The insets show the inverse

susceptibility of the paramagnetic regime. The inverse susceptibility, $1/\chi$, was fitted with a classical Curie–Weiss relation, $\chi = C/(T - \theta)$, in a temperature range that varied depending on the compound. The magnetic parameters are listed in Table 3. An evident ferromagnetic behavior is observed at $x = 0.3$, characterized by a high transition temperature, $T_C = 276.5$ K, and large ZFC and FC ferromagnetic components. For $x = 0.7$, an antiferromagnetic behavior is observed with a Néel temperature T_N equal to 35.2 K, but the positive value of θ (+71,6 K, Table 3) indicates a dominant ferromagnetic character of the exchange interactions (Fig. 5). The sample with $x = 0.7$ presents an irreversible behavior near the transition temperature which suggests a spin glass state similar to the one found in $CuCrSbSe_4$ [34] and $CuCr_xHf_ySe_4$ [15]. The appearance of a spin glass state is probably due to a super-exchange interaction. Indeed, in $CuCr_2Se_4$, the interactions are predominantly ferromagnetic, although both ferromagnetic (nearest neighbor 90° exchange) and antiferromagnetic (next-nearest neighbor) couplings exist. When Cr is substituted by Sn ions, the antiferromagnetic components are promoted, and the ferromagnetic components are partially inhibited and form ferromagnetic clusters. This may be associated with the increase in the length of the Cr-Se bonds that stimulates the antiferromagnetic interaction when the Sn ion content increases, from 2.5458 Å ($x = 0.3$) to 2.5671 Å ($x = 0.5$). This fact changes the orientation of the localized magnetic moments in the samples, and a spin-glass state appears, similar to the one found in $CuCrSbSe_4$ [34] and $CuCr_xHf_ySe_4$ [15]. The observed effective moment for $CuCr_{1.3}Sn_{0.7}Se_4$ ($\mu_{eff} = 4.65$ μ_B) is close to the moment expected for high-spin states: $Cu^{1+}[Cr_{1.0}^{3+}Cr_{0.3}^{4+}]Sn_{0.7}^{4+}Se_4$ ($\mu^{theo} = 4.17$ μ_B).

4. Conclusions

Single crystals of $CuCr_{1.5}Sn_{0.5}Se_4$, $CuCr_{1.7}Sn_{0.3}Se_4$, $CuCr_{1.5}Zr_{0.5}Se_4$ and $CuCr_{1.8}Zr_{0.2}Se_4$ were obtained via conventional solid-state synthesis. Their crystal structures were determined by single-crystal X-ray diffraction and correspond to spinel-type structures. The $Se[M_3Cu]$ tetrahedron is the most distorted polyhedron ($\sim$ 8 % distortion from an ideal tetrahedron). The Raman spectra indicated that the

frequency variations in the $CuCr_2Se_4$ end-member can be attributed to disorder effects related to the chemical substitution of Cr by Zr and Sn. Magnetic measurement performed down to 2 K showed a ferromagnetic behavior for $CuCr_{1.7}Sn_{0.3}Se_4$. At higher Sn-doping ($x = 0.7$) the substitution of Cr by Sn simultaneously weakens the ferromagnetic nearest neighbor exchange between Cr ions and promotes the remaining antiferromagnetic next-nearest neighbor ion interactions with appearance of a spin glass behavior.

Acknowledgments

References

[1] A.P. Ramirez, R.J. Cava, J. Krajewski, Colossal magnetoresistance in Cr-based chalcogenide spinels, Nature 386 (1997) 156–159. doi: 10.1038/386156a0.

[2] S. Krohns, F. Schrettle, P. Lunkenheimer, V. Tsurkan, A. Loidl, Colossal magnetocapacitive effect in differently synthesized and doped $CdCr_2S_4$, Physica B 403 (2008) 4224-4227. doi:10.1016/j.physb.2008.09.024.

[3] V.N. Antonov, V.P. Antropov, B.N. Harmon, A.N. Yaresko, A. Ya. Perlov, Fully relativistic spin-polarized LMTO calculations of the magneto-optical Kerr effect of d and f ferromagnetic materials. I. Chromium spinel chalcogenides, Phys. Rev. B. 59 (1999) 14552–14560. doi: 10.1103/PhysRevB.59.14552.

[4] E.O. Wollan, W.C. Koehler, Neutron Diffraction Study of the Magnetic Properties of the Series of Perovskite-Type Compounds [(1-x)La,xCa]MnO_3, Phys. Rev. 100 (1955) 545-563. doi: 10.1103/PhysRev.100.545

[5] R. von Helmolt, J. Wecker, B. Holzapfel, L. Schultz, K. Samwer, Giant negative magnetoresistance in perovskitelike $La_{2/3}Ba_{1/3}MnO_x$ ferromagnetic film, Phys. Rev. Lett. 71 (1993) 2331–2333. doi: 10.1103/PhysRevLett.71.2331.

[6] K. Das, P. Dasgupta, A. Poddar, I. Das, Significant enhancement of magnetoresistance with the reduction of particle size in nanometer scale, Sci. Rep. 6 (2016) 20351. doi:10.1038/srep20351.

[7]   Y. Fujimoto, T. Fujita, S. Mitsudo, T. Idehara, Y. Kawashima, S. Nagata, High-frequency ESR studies of colossal magnetoresistance system $Cu(Cr_{1-x}Zr_x)_2S_4$, J. Magn. Magn. Mater. 310 (2007) 1991–1993. doi: 10.1016/j.jmmm.2006.11.059.

[8]   F.K. Lotgering, Ferromagnetism in spinels: $CuCr_2S_4$ and $CuCr_2Se_4$, Solid State Commun. 2 (1964) 55-56. doi: 10.1016/0038-1098(64)90573-3.

[9]   T. Saha-Dasgupta, Molly De Raychaudhury, D.D. Sarma, Ferromagnetism in metallic chalcospinels $CuCr_2S_4$ and $CuCr_2Se_4$, Phys. Rev. B 76 (2007) 054441. doi: 10.1103/PhysRevB.76.054441.

[10]   H. Sims, K. Ramasamy, W.H. Butler, A. Gupta, Electronic structure of magnetic semiconductor $CuCr_2Te_4$: A possible spin-dependent symmetry filter, Appl. Phys. Lett. 103 (2013) 192402. doi: 10.1063/1.4827818

[11]   P. Barahona, A. Galdámez, F. López-Vergara, V. Manríquez, O. Peña, Crystal structure and magnetic properties of titanium-based $CuTi_{2-x}M_xS_4$ and $CuCr_{2-x}Ti_xSe_4$ chalcospinels, J. Solid State Chem. 212 (2014) 114–120. doi: 10.1016/j.jssc.2014.01.017.

[12]   K. Belakroum, Z. Ouili, A. Leblanc-Soreau, M. Hemmida, H.A. Krug Von Nidda, Magnetic properties of $CuCrZrSe_4$, J. Magn. Magn. Mater. 334 (2013) 130–135. doi: 10.1016/j.jmmm.2012.12.006.

[13]   H. Yamamoto, Y. Kawashima, K. Hondou, S. Ebisu, S. Nagata, Spin-liquid behavior in the spinel-type $Cu(Cr_{1-x}Zr_x)_2S_4$, J. Magn. Magn. Mater. 310 (2007) e426-e428. doi: 10.1016/j.jmmm.2006.10.437

[14]   Y. Iijima, Y. Kamei, N. Kobayashi, J. Awaka, T. Iwasa, S. Ebisu, S. Chikazawa, S. Nagata, A new ferromagnetic thiospinel $CuCrZrS_4$ with re-entrant spin-glass behaviour, Philos. Mag. 83 (2003) 2521–2530. doi:10.1080/0141861031000109609.

[15]   E. Maciążek, E. Malicka, A. Gągor, Z. Stokłosa, T. Groń, B. Sawicki, H. Duda, A. Gudwański, Semiconducting-metallic transition of singlecrystalline ferromagnetic Hf-doped $CuCr_2Se_4$ spinels, Phys. B: Condens. Matter. 520 (2017) 116–122. doi:10.1016/j.physb.2017.05.049.

[16]   Bruker SMART, SAINTPLUS, Bruker Analytical X-ray Instruments Inc., Madison, Wisconsin, USA, 2000.

[17]   SADABS, Area-Detector Absorption Correction, Siemens Industrial Automation Inc., Madison, WI, USA, 1996

[18]   Bruker APEX3, SAINT, Bruker Analytical X-ray Instruments Inc., Madison, Wisconsin, USA, 2016.

[19]   Blessing, R. H.: An empirical correction for absorption anisotropy, Acta Cryst. A51 (1995) 33-38.

[20]   G. M. Sheldrick: Crystal structure refinement with SHELXL. Acta Cryst. C71 (2015) 3-8.

[21]   H. Dolomanov, O.V.; Bourhis, L.J.; Gildea, R.J.; Howard, J.A.K.; Puschmann, Olex 2: A complete structure solution, refinement and analysis program, J. Appl. Cryst. 42 (2009) 339-341. doi: 10.1107/S0021889808042726.

[22]   A.L. Spek, Single-crystal structure validation with the program PLATON, J. Appl. Cryst. 36

(2003) 7-13. doi: 10.1107/S0021889802022112.

[23] I. Okonska-Kozlowska, J. Kopyczok, H.D. Lutz, T. Stingl, Single-crystal structure refinement of spinel-type $CuCr_2Se_4$, Acta Cryst. C49 (1993), 1448–1449. doi:10.1107/S0108270193001945.

[24] Von S. Strick, G. Eulenberger, H. Hahn, Über einige quaternäre Chalkogenide mit Spinellstruktur, Z. Anorg. All. Chem. 357 (1968) 338-344. doi: 10.1002/zaac.19683570421.

[25] D. Mähl, J. Pickardt, B. Reuter, Züchtung und untersuchung von einkristallen der verbindungen $CuCrZrSe_4$ und $CuCrSnSe_4$, Z. Anorg. Allg. Chem. 508 (1984) 197–200. doi: 10.1002/zaac.19845080128.

[26] R.D. Shannon, Revised effective ionic radii and systematic studies of interatomic distances in halides and chalcogenides, Acta Cryst. A32 (1976) 751–767. doi: 10.1107/S0567739476001551.

[27] W.H. Baur, The geometry of polyhedral distortions. Predictive relationships for the phosphate group, Acta Cryst. B30 (1974) 1195–1215. doi: 10.1107/S0567740874004560.

[28] M. Wildner, On the geometry of $Co(II)O_6$ polyhedra in inorganic compounds, Z. Kristallogr. 202 (1992) 51–70. doi: 10.1524/zkri.1992.202.14.51.

[29] K. Robinson, G.V.Gibbs, P.H. Ribbe, Quadratic elongation: a quantitative measure of distortion in coordination polyhedra, Science 172 (1971) 567–570. doi: 10.1126/science.172.3983.567.

[30] V.G. Ivanov, M.N. Iliev, Y.-H.A. Wang, A. Gupta, Ferromagnetic spinel $CuCr_2Se_4$ studied by Raman spectroscopy and lattice dynamics calculations, Phys. Rev. B 81 (2010) 224302. doi: 10.1103/PhysRevB.81.224302.

[31] M. Iliev, G. Güntherodt, H. Pink, Resonant Raman scattering of $CdCr_2Se_4$, Solid State Commun. 27 (1978) 863–866. doi: 10.1016/0038-1098(78)90193-X.

[32] K. Fajans, Struktur und deformation der Elektronenhüllen in ihrer Bedeutung für die chemischen und optischen Eigenschaften anorganischer Verbindungen, Die Naturwissenschaften, 11 (1923) 165–172. doi: 10.1007/BF01552365.

[33] I. Jendrzejewska, P. Zajdel, J. Mroziński, E. Maciążek, T. Goryczka, A. Hanc, A. Kita, X-ray investigations and magnetic properties of $CuCr_{2-x}Sn_xSe_4$ - compounds, Solid State Phenom. 163 (2010) 208–212. doi: 10.4028/www.scientific.net/SSP.163.208.

[34] J. Krok-Kowalski, J. Warczewski, P. Gusin, T. Śliwińska, G. Urban, E. Malicka, A. Pacyna, T. Mydlarz, P. Rduch, G. Władarz, Antimony valence and the magnetization processes in the spinels $(Cu)[CrSb]Se_4$, J. Alloy. Compd. 478 (2009) 14–18. doi:10.1016/j.jallcom.2008.11.021.

Figure captions

Figure 1: Crystal structure of Selenospinels of general chemical formula $CuCr_{2-x}M_xSe_4$. The copper (cyan sphere) is coordinated by selenium atoms (yellow spheres). The chromium and M metals ($M = Sn$, Zr) randomly occupy the 16d Wyckoff site (green spheres).
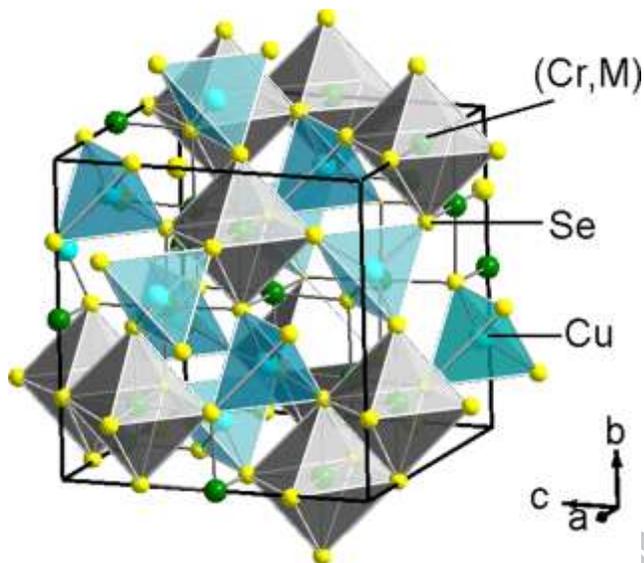

Figure 2: Vegard´s law from single-crystals data: (**Top**) $CuCr_{1.7}Sn_{0.3}Se_4$ and $CuCr_{1.5}Sn_{0.5}Se_4$; (**Bottom**) $CuCr_{1.8}Zr_{0.2}Se_4$ and $CuCr_{1.5}Zr_{0.5}Se_4$. The a lattice parameters of $CuCr_2Se_4$, $CuCrZrSe_4$ and $CuCrSnSe_4$ are included.
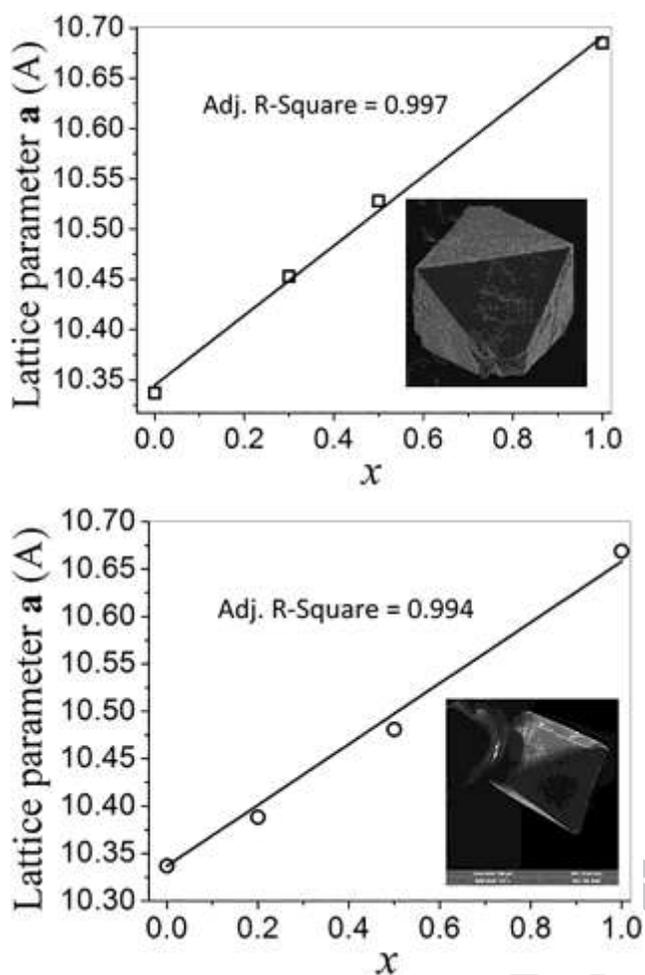
Figure 3: Scanning electron microscopy (SEM) micrograph: Backscattering electron image of $CuCr_{1.8}Zr_{0.2}Se_4$ and an example of EDS mapping spectral analysis (20 kV, 6696x).

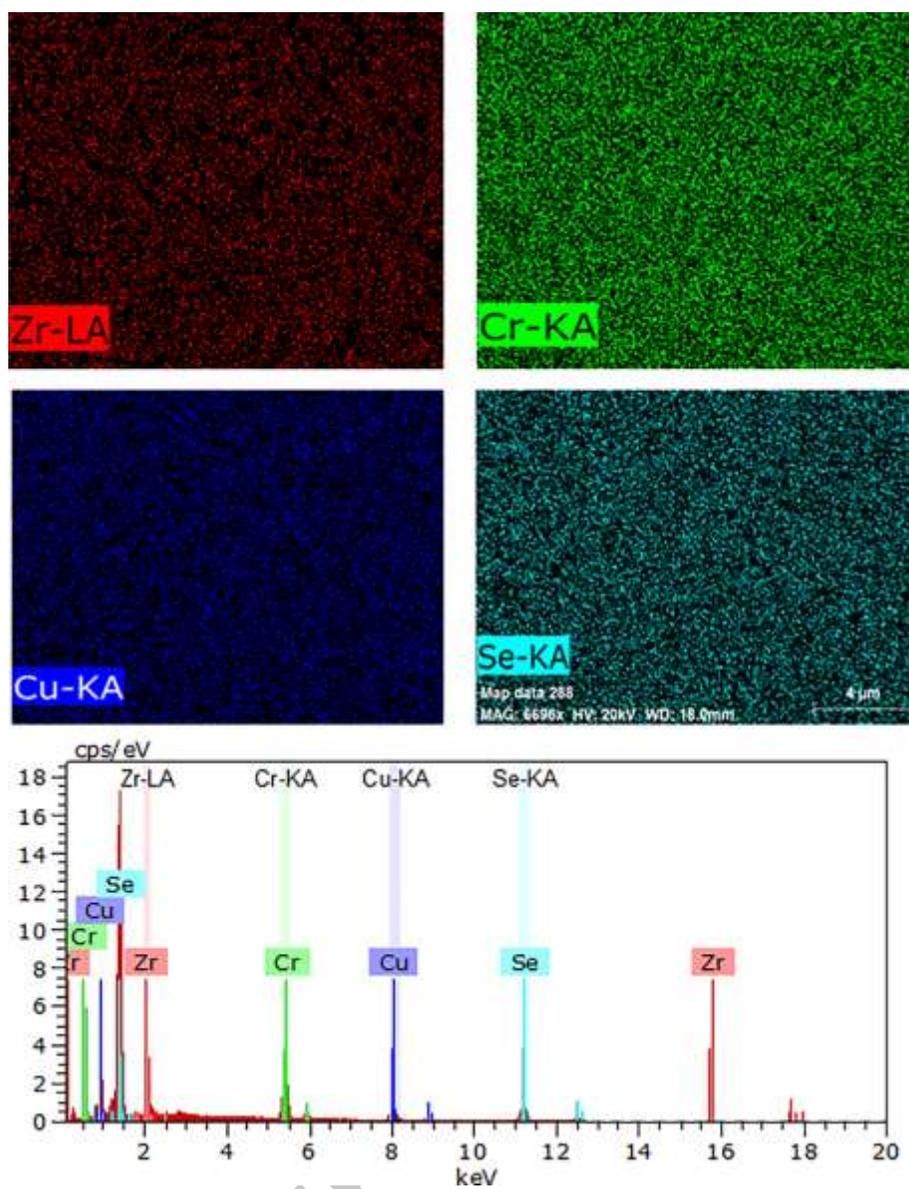**Figure 4:** Single-crystal Raman spectra of (**a**) CuCr$_{1.5}$Zr$_{0.5}$Se$_4$, (**b**) CuCr$_{1.8}$Zr$_{0.2}$Se$_4$, and (**c**) CuCr$_{1.5}$Sn$_{0.5}$Se$_4$.

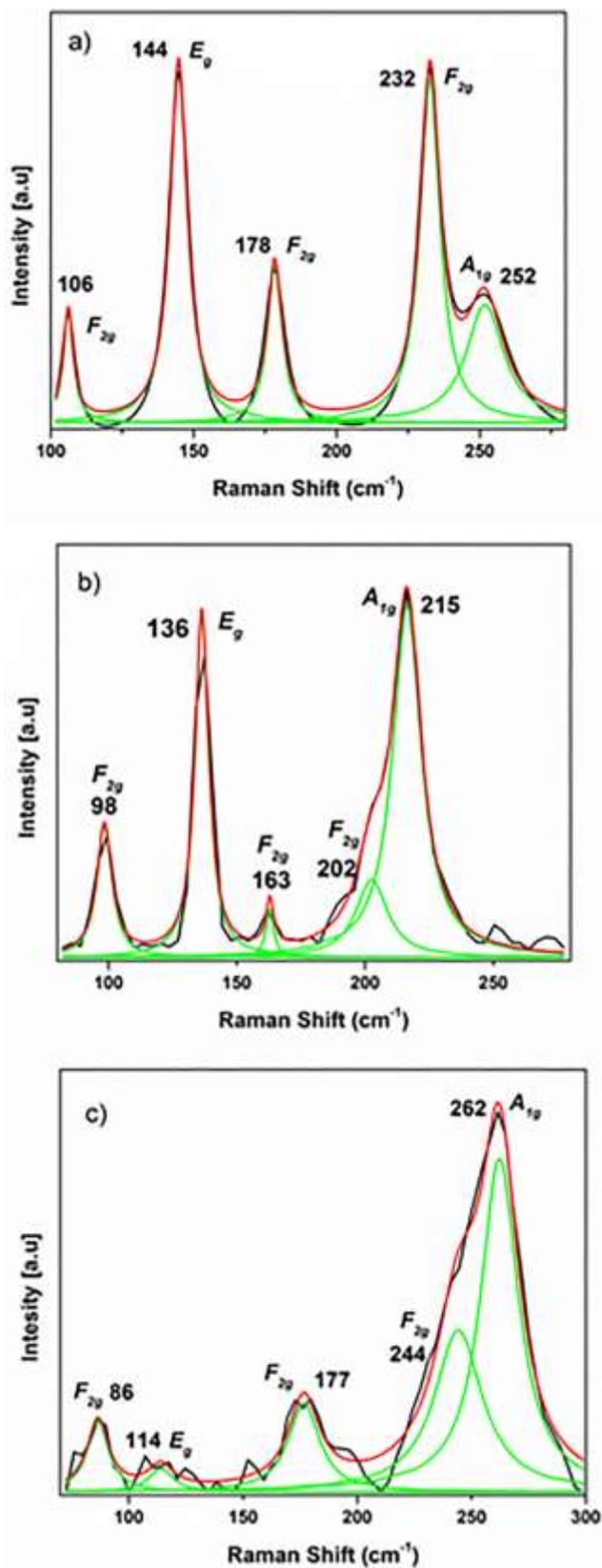**Figure 5:** ZFC/FC magnetization cycles measured at H_{app} = 500 Oe for a powder sample of $CuCr_{1.7}Sn_{0.3}Se_4$. The insert shows the $1/\chi$-*versus*-temperature behavior fitted by a Curie-Weiss law.

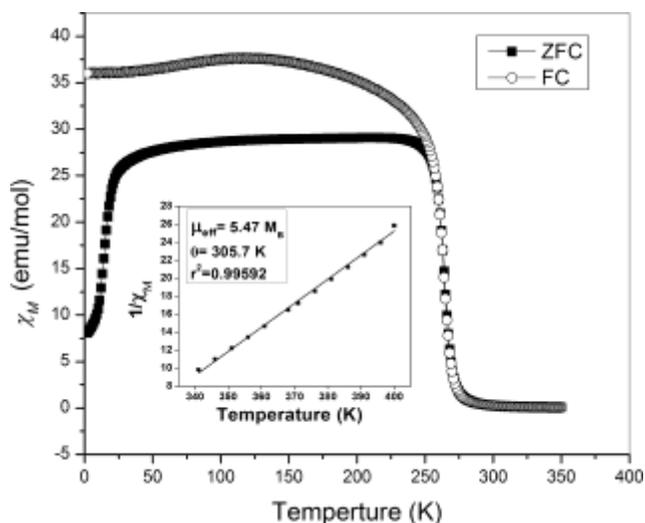**Figure 6:** ZFC/FC magnetization cycles measured at H_{app} = 500 Oe for a powder sample of $CuCr_{1.3}Sn_{0.7}Se_4$. The insert shows the $1/\chi$-*versus*-temperature behavior fitted by a Curie-Weiss law.

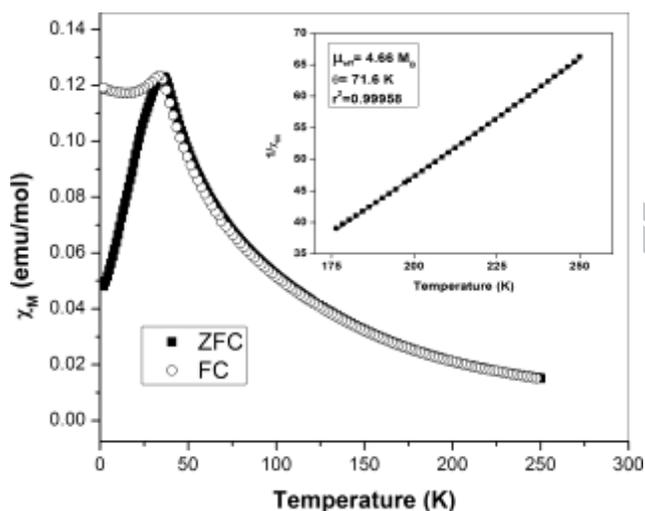**Table 1**: Crystallographic data and structure refinement details for $CuCr_{2-x}M_xSe_4$.

	$CuCr_{1.8}Zr_{0.2}Se_4$	$CuCr_{1.5}Zr_{0.5}Se_4$	$CuCr_{1.7}Sn_{0.3}Se_4$	$CuCr_{1.5}Sn_{0.5}Se_4$
Crystal data				
Crystal Size (mm)	0.28×0.18×0.16	0.16×0.14×0.11	0.25×0.18×0.15	0.21×0.19×0.12
Crystal System, Space Group			Cubic, Fd-3m	
Unit cell dimension *a* (Å)	10.3883(12)	10.4807(12)	10.4530(10)	10.5279(10)
Cell volume (Å^3)	1121.1(2)	1151.3(4)	1142.15(3)	1166.9(3)

Data Collection

Temperature (K)	293 (2)			
Wavelength (Å)	Mo Kα, 0.71073	Cu Kα, 1.54178	Mo Kα, 0.71073	Mo Kα, 0.71073
Absorption coefficient (mm^{-1})	33.367	62.240	33.517	33.273
θ-range (°)	$3.97 <θ< 27.65$	$12.0 <θ< 86.14$	$3.38 <θ< 30.21$	$3.35 <θ< 29.13$
hkl-range	$-13 <h< 13$	$-12 <h< 13$	$-14 <h< 14$	$-14 <h< 14$
	$-12 <k< 13$	$-13 <k< 13$	$-14 <k< 14$	$-13 <k< 14$
	$-13 <l< 13$	$-13 <l< 12$	$-14 <l< 14$	$-14 <l< 14$
No. of reflections	2089	3774	2600	2598
R_{int}, R_{σ}	0.0325,0.0105	0.0525, 0.0105	0.0507, 0.0166	0.0542,0.0180
No. of independent reflections	85	84	106	107

Refinement

Refined method	Full-matrix least-squares on F^2			
No. of parameters	8	8	8	8
Extinction coefficient	0.00029 (8)	0.000126(16)	0.00069 (7)	0.00067(5)
R_1 (I>2σ$_I$), R_1 (all)	0.0195, 0.0197	0.0239, 0.0264	0.0200, 0.0221	0.0174, 0.0200
wR_2 (I > 2σ$_I$), wR_2(all)	0.0632,0.0633	0.0587, 0.0596	0.0483, 0.0487	0.0376, 0.0382
Goodness-of- fit F^2	1.233	1.200	1.197	1.116
Δρmax, Δρmin (e Å^{-3})	0.726, -0.839	1.251, -1.340	0.606, -0.792	0.482, -0.551

Table 2: Anionic *u* parameters and equivalent isotropic displacement parameters for CuCr$_{2-x}$M$_x$Se$_4$ (M = Zr, Sn)

Compound	Anion *u* parameter	U_{eq} (Å^2)§		
		Cu*	Cr/M*	Se*
CuCr$_{1.8}$Zr$_{0.2}$Se$_4$	0.25697(5)	0.0112 (6)	0.0090 (6)	0.0077 (4)

$CuCr_{1.5}Zr_{0.5}Se_4$	0.25632(4)	0.0165 (5)	0.0114 (4)	0.0110 (4)
$CuCr_{1.7}Sn_{0.3}Se_4$	0.25663(4)	0.0083 (4)	0.0055 (3)	0.0089 (3)
$CuCr_{1.5}Sn_{0.5}Se_4$	0.25632(3)	0.0111 (3)	0.0098 (2)	0.0126 (2)

[§]U_{eq} is defined as one third of the trace of the orthogonalized U_{ij} tensor

* Cu in A site (8a); Cr/Zr/Sn in B site (16d) and Se in Anion site (32e)

Table 3: Magnetic parameters for seleno-spinel compounds.

Compound	T_C[$]^{\$}$, T_N[*] (K)	μ_{eff} (μ_B)	θ (K)
$CuCr_{1.7}Sn_{0.3}Se_4$	276.5	5.47	+ 305.7
$CuCr_{1.3}Sn_{0.7}Se_4$	35.2	4.66	+ 71.6

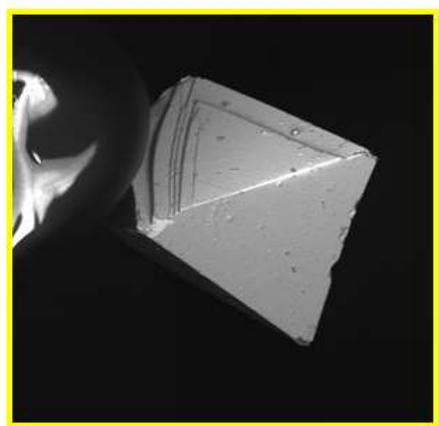$: T_C determined by extrapolation to the T-axis of the steepest slope of the FC magnetization

*: T_N corresponds to the temperature of the maximum of the susceptibility.
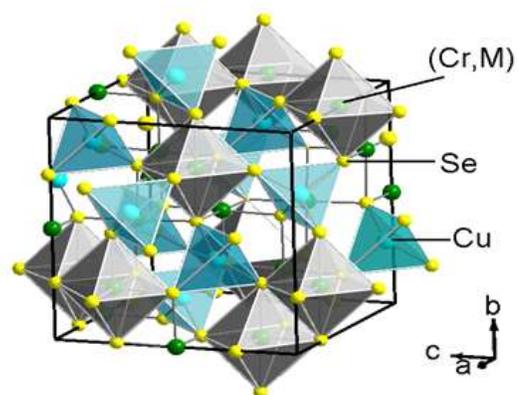
*Research Highlights

- $CuCr_{2-x}Zr_xSe_4$ and $CuCr_{2-x}Sn_xSe_4$ belong to the family of spinel-type compounds
- Analysis of Raman spectral features of main peaks from $CuCr_{2-x}M_xSe_4$ (M = Zr, Sn)
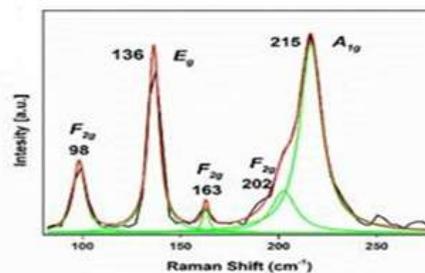- Ferromagnetic and spin-glass behavior

*Graphical Abstract Legend

Single-crystal of $CuCr_{1.8}Zr_{0.2}Se_4$, asymmetry unit with polyhedral representation and Raman scattering spectra performed on single-crystal.